Use of X-ray Microscopy and Synchrotron Microtomography To Characterize Polyethylene Polymerization Particles

W. Curtis Conner,*,† Steven W. Webb,† Per Spanne,‡ and Keith W. Jones‡

Department of Chemical Engineering, University of Massachusetts, Amherst, Massachusetts 01003, and Atomic and Applied Physics Group, Brookhaven National Laboratory, Upton, New York 11973

Received March 5, 1990; Revised Manuscript Received April 12, 1990

ABSTRACT: Many models have been proposed for heterogeneous polymerization kinetics that make varying assumptions regarding the catalyst fragment sizes and their distribution within the growing particles. An understanding of the processes of catalyst fragmentation, fragment dispersion, and particle agglomeration is crucial in the design of heterogeneous, olefin polymerization catalysts. Each of these phenomena can profoundly influence the course of the polymerization and the properties of the final polymer product. The phenomena and their influence on catalyst disintegration within the growing polymer particle have not, heretofore, been studied directly. We have employed high-resolution (to 5 μm) synchrotron computed microtomography, using the X26C beamline at Brookhaven National Laboratory, to directly image the distribution of larger silica fragments and voids within single polymer particles at varying polymer yields. These samples had been prepared by gas-phase ethylene polymerization over silica-supported chromium catalysts to yields of 11–200 g of polymer/g of catalyst. We come to several conclusions from these studies: (1) the catalyst fragment distribution is not uniform within the particles (the discernable larger fragments are concentrated near the periphery of the particles), (2) large fragments (>30 μm) are still evident at yields up to 200 g/g, and (3) the particles comprise at least 20–30% voids of dimensions >50 μm.

Introduction

It is a major objective of polymerization catalyst design for heterogeneous polymerization to understand the process of catalyst fragmentation and polymerizing particle agglomeration during polymerization. Both phenomena have profound influences on the course of the polymerization and the properties of the final polymer product. We have observed that effective catalyst fragmentation is essential to maintaining the polymerization reaction against an increasing mass transport resistance due to the expanding and encapsulating polymer phase. If the particles do not fragment by several orders of magnitude, the polymerization becomes severely diffusion limited and eventually the reaction ceases.

Even if fragmentation occurs, monomer must efficiently diffuse to the active catalyst surface to maintain the polymerization. The transport is complicated by the multiphase nature of the polymer particle; monomer must diffuse through the polymer particle around voids and through the polymer-filled pores of the catalyst fragments to the active sites on the fragment surfaces. The spatial distribution of catalyst fragments throughout the polymer particles, fragment size, and morphology are important influences in the potential diffusion control of the process. Extensive polymer particle agglomeration and lack of catalyst friability leads to polymer particles containing large catalyst pieces as well as lowering the polymerization rate, polymer particle density, and ultimate polymer yield.

The phenomena, and influence, of catalyst disintegration within the polymer particle during polymerization has never been experimentally addressed before. Many models have been proposed for catalytic polymerization kinetics that make varying assumptions regarding the catalyst fragment size and distribution within the polymer particle. Floyd et al.[1] completely ignore fragmentation and tacitly assume fragments are negligibly small and uniformly distributed. Chiovetta[2] uses a single-particle analysis of fragmentation but does not describe how the fragmented pieces are convected throughout the polymer particle at high polymer yields. These models are mainly directed at the titanium/chloride supported systems in which friability is known to be great and the influence of fragmentation dynamics is perhaps not limiting.

In the silica-supported systems, fragmentation dynamics cannot be disregarded in the analysis of the polymerization kinetics. We[3] have shown that the influence of diffusion during the nascent polymerization is significant and can increase with inhibited fragmentation of the silica phase and agglomeration of polymer particles. It was assumed in this work that fragments are relatively uniformly dispersed throughout the polymer particle. The effective monomer transport length was based on the polymer particle size. However, at high polymer yields the distribution and size of fragments within the polymer particles is not known. It is conventional to assume, without any experimental evidence or validation, catalytic sites and fragments are uniformly distributed within the polymer particle.

Models by Schmeal and Street[4] and Singh and Merrill[5] postulate that fragments may be distributed in three ways: (1) a "hard-core" model in which polymerization occurs around a center catalyst particle, which is nonfriable, (2) "uniform" site model in which fragments are small and uniformly distributed within the particle, and (3) "expanding-core" model in which fragments are convected to the exterior particle surface by internal expansion. The models are diagrammed in Figure 1. Each model must assume a different mechanism for catalyst disintegration and has different implications for the influence of monomer transport on the kinetics.

For instance, the hard-core model assumes no fragmentation and would predict a slowly decreasing rate of polymerization with polymer accumulation simply due to the increasing transport length. This model is perhaps applicable to nonfriable catalysts or extensive particle agglomeration. The uniform and expanding-core models both assume friability but recognize different convection mechanisms. The uniform model implicitly assumes that

† University of Massachusetts.
‡ Brookhaven National Laboratory.

0024-9297/90/2223-4742$02.50/0

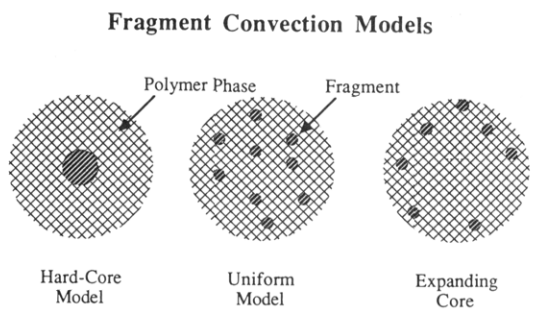

Figure 1. Models for the convection of catalyst fragments within an expanding polymer particle.

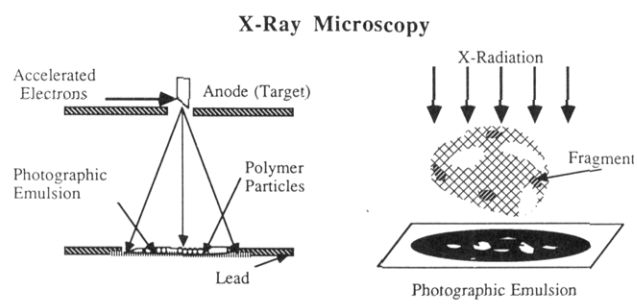

Figure 2. Set-up of X-ray and a sample for X-ray microscopy.

catalyst fragmentation is uniform and complete early in the polymerization. Polymer grows around each small catalyst crystallite at roughly equal rates, resulting in uniform convective forces on each crystallite and a uniform dispersion within the polymer particle. If, however, some fragments were less active than others (e.g., larger due to nonuniform catalyst disintegration), these fragments would be convected away from the smaller crystallites due to differential expansion. Larger fragments would be convected to the polymer particle surface where they would become more monomer accessible. If fragmentation occurs nonuniformly, then some combination of models (uniform and expanding core) would be necessary.

The presence of voids in the polymer particles is highly undesirable since it increases the cost of shipping of the polymer. Voids arise from two processes: (1) agglomeration during nascent polymerization and (2) nonuniform fragmentation. Both issues are significant during the crucial nascent period of the polymerization reaction. Agglomeration is difficult to avoid since the nascent polymerization is highly exothermic and the catalyst particle is thermally insulative. Dilution of either the monomer or solids phase is the normal precaution used to prevent uncontrollable aggregation of polymer particles. Nonuniform fragmentation (e.g., excessively fast fragmentation or fragmentation by attrition rather than progressive particle subdivision) can rapidly increase the concentration of small, overheated particles and exacerbate the aggregation problem during nascent polymerization. Incomplete or delayed fragmentation can lead to prolonged exotherms, increasing the possibility of agglomeration.

Clearly, an experimental technique that describes fragment and void size and location within the polymer particle as a function of polymer yield is needed. Heretofore, no such technique existed. No technique has been found to study the size and spatial distribution of catalyst fragments without substantially modifying the system in some manner. Isolation of fragments by removal of the polymer phase (by plasma ashing, solvent extraction, and combustion) was only modestly successful and is only feasible for polymer particles of relatively low polymer content (Weist et al.[6]). Polymer removal is not practical for polymer contents greater than 5–10 g/g of catalyst. It is not clear that fragments isolated by removal of the polymer are representative of the fragments that actually exist within the polymer particle.

We will describe a new technique to study the morphology (catalyst fragments, polymer and void structures) of the growing polymer/catalyst particles at intermediate polymer yields of less than 1 kg/g. This technique provides detailed new insight into the mechanism of catalytic polymerization and catalyst fragmentation with silica-supported catalysts. It also demonstrates the developing utility (and increasing sensitivity) of computed microtomography using the National Synchrotron Light Source (NSLS) at Brookhaven National Laboratory.

We employ two techniques to image the polymerization particles: (1) X-ray microscopy (XRM) and (2) X-ray computed microtomography (μCT). Particles directly from the polymerization reactor can be examined with no additional preparation. Both techniques are nondestructive and provide a view of the fragments as they exist within the polymer particle. With this information, fragmentation of the silica phase and aggregation of the polymer phase during polymerization are more directly characterized.

X-ray microscopy was performed by using a simple X-ray tube and optical enlargement of the developed image on photographic film. XRM provides a projection of the X-ray absorption within a single particle and thus gives a 2D representation of fragment or void size and location within the polymer particle. 3D information about void and fragment phases within polymer particles is not easily extracted from XRM projection images.

μCT was performed by using synchrotron X-rays and computer image reconstruction and analysis. In contrast to XRM, computed tomography has the capability to noninvasively image the X-ray absorption properties (the linear attenuation coefficient) within thin transverse slices through the particle. Thus, μCT images are a more direct representation of the spatial position of catalyst pieces within the particle. Several such slice images within a single particle can create a true 3D representation of size, position, and orientation of the various phases that comprise the polymer particle.

Although μCT using conventional X-ray sources has been reported (e.g., Sato et al.;[7] Carlsson et al.;[8,9] Elliott and Dover;[10] Sequín et al.[11]), this new field of imaging has its greatest potential at synchrotron X-ray sources since very intense radiation sources are required (e.g., Grodzins;[12] Flannery et al.;[13] Spanne and Rivers;[14,15] Kinney et al.;[16,17] Jones et al.;[18–20]; Nichols et al.;[21] Sakamoto;[22] Jones et al.;[23] Spanne[24]). Further, the advantages of synchrotron radiation for μCT are its low divergence and the possibility of energy tuning using X-ray monochromators. Thus, imaging with vastly improved spatial resolution (down to the micrometer range), high contrast, and fast data collection can be achieved relative to laboratory X-ray sources.

Experimental Section

X-ray Microscopy. The XRM source was 10–100 kV at 60-mA current (Klystron X-ray tube, Field Emission Corp). It has a focal spot size of 500 μm and a maximum focus-to-film distance of 60 cm. The beam diverges at 30°; at 60 cm, the beam covers a circle of radius 30 cm.

Samples of the polymer particles after polymerization were spread in a single particle layer between two sheets of clear *adhesive tape (~50-μm thickness) and sealed to prevent* contamination by dust (Figure 2). The sample was placed on top of a sheet of bare X-ray film (Kodak DEF high resolution; 5 in.; quoted resolution ~400 lines/mm or 2.5 μm), emulsion side up,

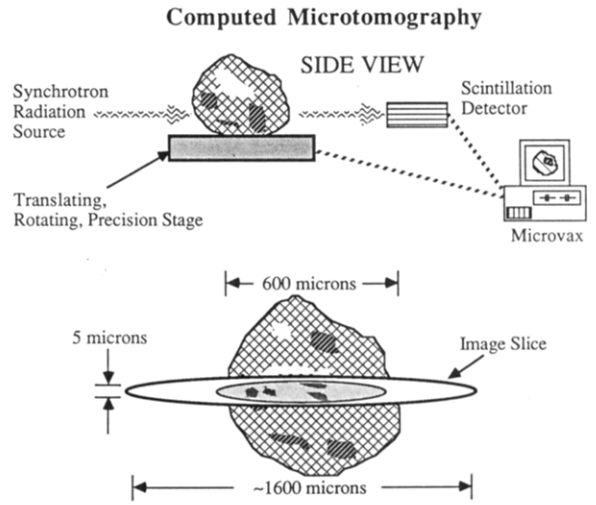

Figure 3. Set-up of X-ray microtomographic imaging system: Beam X26C-NSLS at Brookhaven National Laboratory, Upton, NY.

and bordered by lead foil. X-ray exposure and subsequent film processing was done in a dark room. Power was set at 10 kV (a very low setting for normal X-ray operations). Exposure time was normally 120 s. The combination of power setting, current, and exposure time determines image properties of contrast and brightness. Sample–beam geometry, sample size, sample–film distance, and film quality determine spatial resolution.

X-ray Computed Microtomography. μCT analysis of polyethylene particles was performed by using the high-resolution μCT equipment at the X26C Microprobe Beamline at the National Synchrotron Light Source at Brookhaven National Laboratory (cf. Spanne and Rivers,[14,15] Jones et al.[18,19]). A pencil beam of X-rays was defined by using two crossed tantalum slits. The beam size was 12×5 μm^2. A 1-mm-thick CaF_2 scintillation detector operated in current mode was used to detect transmitted radiation. The samples (single polymer particles with diameters ranging from 700 μm down to about 200 μm) were attached with double-sided tape to a mount on a precision, remote, computer-controlled stage capable of controlled rotation and translation with micrometer precision.

There are two parts of a tomographic imaging experiment: (1) 2D (radial, r, and azimuthal, ϕ) scanning of the particle across a single transverse slice and (2) reconstruction of the r–ϕ slice data into the density variation inside the slice (Figure 3). Transmission measurements were made at 254 equally spaced angles from 0 to 179.63 (increment 0.71). At each angle 160 measurements with a spacing of 10 μm were performed. This is the optimum number of angles in relation to the number of measurements for each angle. The slice thickness, 5 μm, was defined by the beam height. The data collection time was 15 min.

In X-ray absorption μCT the line integrals of the linear attenuation coefficient are used to reconstruct the 2D distribution of the X-ray absorption in the imaged slice. They can be derived from measurements of the relative number of transmitted photons. In this study we used the detector signal as a relative measure of the transmitted number of photons even though it was operated in a mode where the signal depends on the photon energy. This is a reasonable approximation since the objects imaged here were of low contrast.

The image reconstruction program used a filtered back-projection algorithm to reconstruct the 2D distribution of the X-ray absorption in the imaged slice from the 41 000 line integrals. Reconstruction of a single slice required about 15 min a MicroVAX-II computer. Repetition of the imaging for several slices through a particle leads to a 3D representation of the linear attenuation coefficient within a single polymer particle.

Polyethylene Particles. Polymer particles of yields ranging from 0.0 to 200 g/g were X-rayed. Polymer particles were obtained from a high-pressure (7.0 atm of ethylene) stirred bed reactor operated at 95 °C by using a chromium/silica catalyst obtained from Phillips Petroleum and known to be active and friable (Weist et al.[6]).

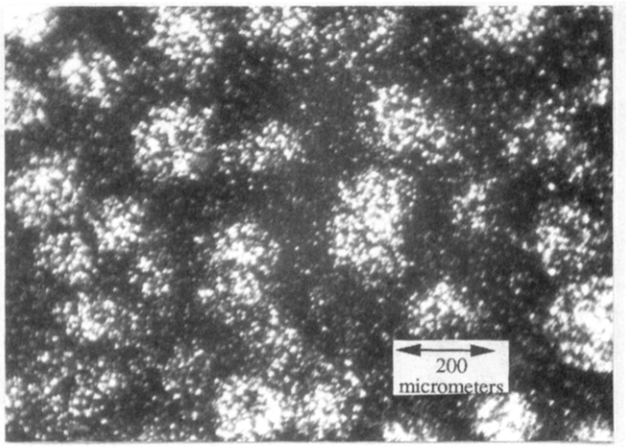

Figure 4. XRM image of polymer particles of size 200 μm and yield 0.8 g/g.

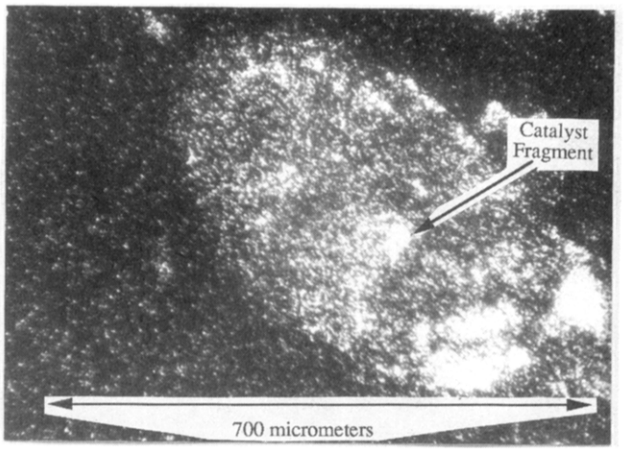

Figure 5. XRM image of a single polymer particle of size 670 μm and yield 200 g/g.

Results

An XRM image of polymer particles of diameter 200 μm after 0.8 g/g of polymer accumulation (i.e., insignificant polymer phase) is shown in Figure 4. Very little catalyst fragmentation and separation is evident at this low polymer yield. The spotty nature of the particle images demonstrates the porosity (>0.5 μm) of the silica support.

Figure 5 depicts an XRM image showing the spatial distribution and size of the fragments dispersed in a single high-yield (200 g/g) polymer particle of size 600 μm. This image demonstrates a lack of contrast between polymer, void, and silica phases within the particle. Spatial resolution was limited by the geometry of the diverging beam and sample thickness and was evaluated to be 5–10 μm.[25] However, the presence of large fragments (white areas) inside the polymer particles is clearly evident. Most of the largest fragments are located near the external boundaries of the polymer particle. Smaller fragments are more randomly distributed within the polymer particles.

Individual particles from the sample with 200 g/g yield (as represented above) were studied by tomography during our initial studies. Figure 6 shows three tomographic slices from a single polymer particle, each parallel but separated spatially within the polymer particle by 100 μm (the last image is near the bottom of the particle). The images represent the density variation across the particle within a slice ~5 μm thick at a spatial resolution of 5–7 μm (given by the dimension of the collimated X-ray beam). The field of view is 1600 μm in diameter. In the images the brightest spots are silica, gray is polymer, and the darkest areas within the particle are voids.

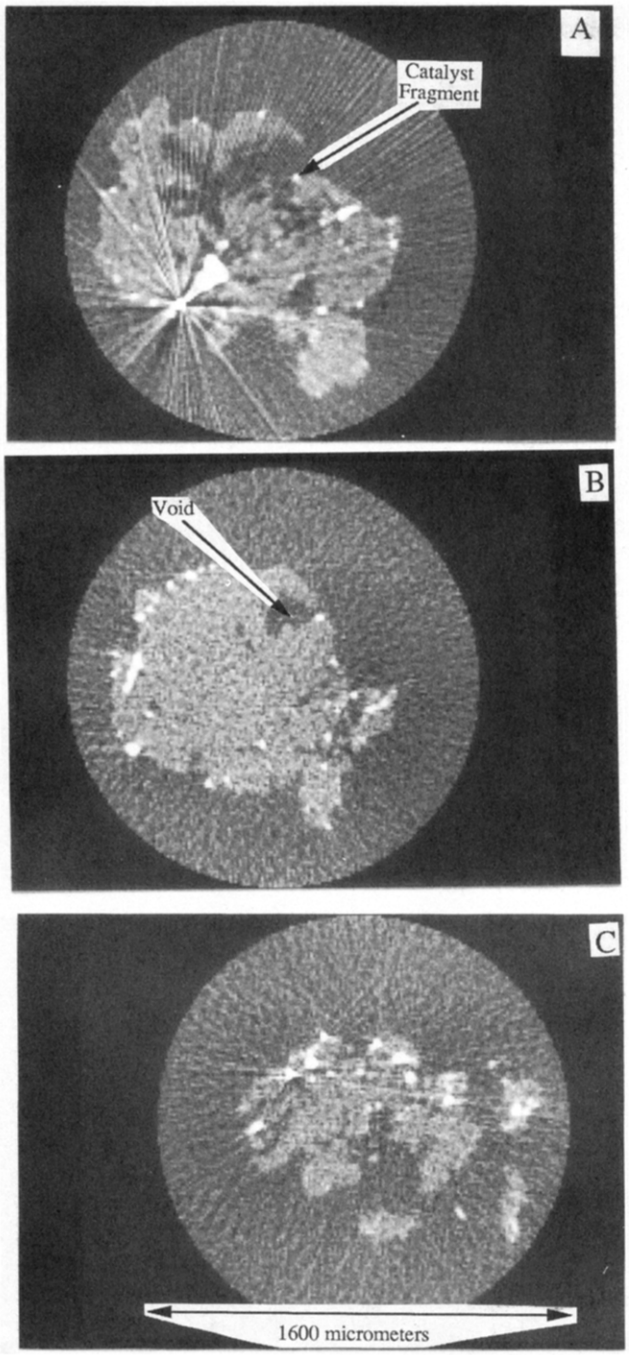

Figure 6. X-ray tomographic images of a single polymer particle of yield 200 g/g: (A)–(C) are each separated by 100 μm within the particle; (C) is near the bottom of the particle.

Images obtained by μCT are far superior to XRM (with our X-ray instrument); contrast and image clarity are much improved. The μCT images represent a thin slice within the particle as contrasted with the two-dimensional projection of density through the particles as represented in the XRM studies. Voids in the polymer particle are clearly seen, as well as the distribution and size of individual fragments within the particle. Voids comprise, in some slices near the particle edges, 50–60% of the particle. When mercury porosimetry (Webb[25]) is used, the total average porosity of these particles is 20–30% v/v, mainly in pores of >20 μm. These μCT slices attest to the irregular, three-dimensional, multiphase nature of the polymer particle. These images show that this porosity is nonuniformly distributed within the particle. This may be evidence of random agglomeration of polymerizing particles of different sizes or highly nonuniform fragmentation during polymerization.

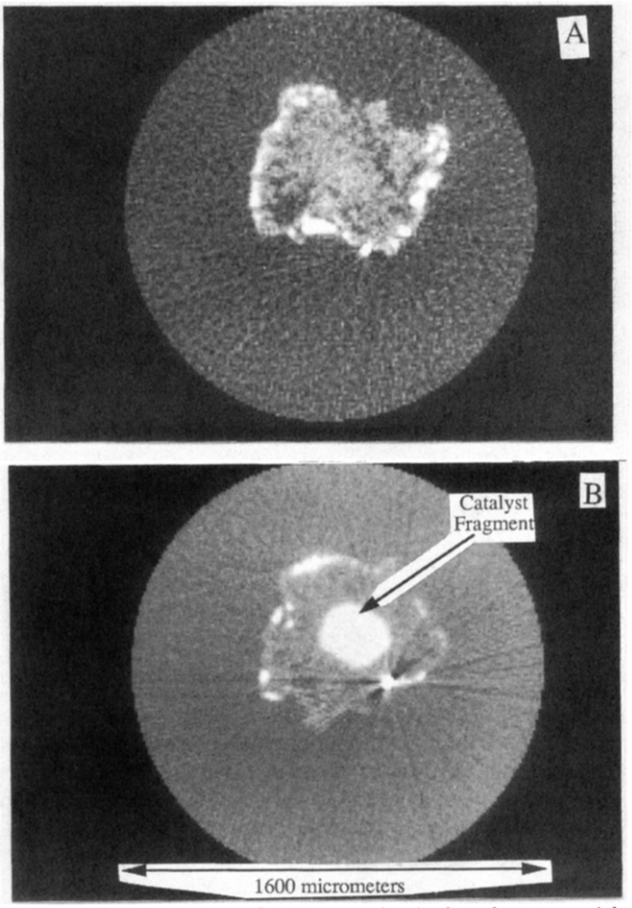

Figure 7. X-ray tomographic images of a single polymer particle of yield 50 g/g: (A) and (B) are separated by 100 μm within the particle.

The only difficulty with μCT of these samples was the appearance of so-called particle volume artifacts in the reconstructed images. They arise when very large differences in the linear attenuation coefficient are present and appear as "exploding star" defects in some of the images. We believe the dense spots are steel fragments from the reactor surfaces incorporated into the polymer particle during polymerization.

Only catalyst fragments of size >3 μm are definitively resolved in the μCT images. As inferred from the XRM images, almost every resolved catalyst fragment is located near the boundary of the polymer–void phase. However, μCT clearly shows that the 100 μm fragments resolved in XRM images are not realistic measures of fragment dimension and are probably the projections of 10–50 μm fragments concentrated near the exterior surfaces. μCT is a superior imaging technology compared to XRM.

Figure 7 shows two tomographic images (separated spatially by 100 μm) for a particle of size ~500 μm with a lower polymer yield of 50 g/g. The field of view is kept constant at 1600 μm diameter. Clearly, a much larger catalyst piece (~200 μm) is observed in one slice, and, in general, visible fragments are larger than those found in particles of 200 g/g yield (Figure 6), which may mean that fragmentation is still continuing, even at 50 g/g yield. These images also show that most large fragments are again mainly at the outer edges of the polymer particle. The very large piece is perhaps a nonfriable or inactive catalyst fragment.

Figure 8 shows tomographic images for a collection of 3–5 polymer particles of average yield 11 g/g. These

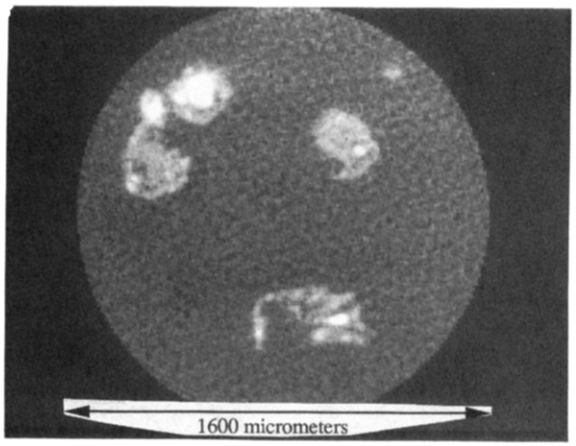

Figure 8. X-ray tomographic images of a several polymer particles of average yield 11 g/g.

particles are of diameter 200 μm and are too small to be easily mounted and imaged. Even at this low yield, a significant polymer phase is observed, as well as large catalyst pieces.

Analysis and Conclusions

X-ray microscopy and computed microtomography have been performed on polyethylene polymerization particles with varying but low amounts of polymer and containing significant residual catalyst. X-ray tomographic imaging allows definition of fragment and void size as well as spatial distribution within a single polymer particle.

The major observations from this imaging work are (1) the fragment distribution within the particle is not uniform (the larger fragments concentrate near the exterior surfaces of the polymer particles), (2) large fragment pieces of size 30–80 μm are evident at a yield of 200 g/g, and (3) the polymer particle is at least 20–30% voids of size >50 μm. These observations may be specific to the polymerization reaction system (e.g., heat transfer and poisoning) and/or catalyst (pore morphology and chromium content) studied. These results indicate that fragmentation and convection of catalyst fragments within the polymer phase are important in determining the transport length scale. They also prove the utility of a new imaging technology that will aid in the understanding and design of improved polymerization catalysts.

Fragmentation Mechanism. Polymerization produces catalyst fragments of vastly differing sizes. This is probably due to some combination of transport limitations during nascent polymerization, aggregation of overheated polymer particles during nascent polymerization, and a nonuniform void morphology of the catalyst itself. A fragment size distribution and large fragments (>5 μm) within the polymer particle are highly undesirable. They compromise polymerization activity and contaminate the polymer product.

It is as yet not clear why larger fragments of silica are convected to the exterior polymer surface. However, we suggest two possibilities:

(1) Larger fragments are less active (i.e., greater transport resistance) than smaller fragments (not visible in these μCT images) located uniformly throughout the particle. Polymerization and polymer expansion convects larger fragments away from the smaller fragments to the exterior surfaces. This is a variation of the expanding-core and uniform models.

(2) Polymer–polymer interaction at temperatures close to the polymer melting point could naturally cause phase segregation, drawing the polymer toward the center and isolating the phase containing the catalyst fragments.

Void Generation. Voids in the polymer particles are also clearly evident in both X-ray imaging techniques and porosimetry. Voids are undesirable since they reduce the particle density of the product. These voids may be created by (1) agglomerative processes that occur between overheated particles (this could be due to too rapid a polymerization rate or a high concentration of overheated, small particles) and (2) spatially disparate polymer formation within a partially disintegrated particle.

The consequences of these studies on the understanding of ethylene polymerization kinetics are significant. Clearly, kinetic models based on uniformity of active sites within the expanding polymer phase (such as Thiele modulus formulations) are not universally applicable and need to be modified. The monomer and heat transport length may be much smaller than the overall particle size. The assumption of a transport length during polymerization must include not only the kinetics of catalyst fragmentation and polymer particle agglomeration but also fragment convection and phase segregation throughout the expanding polymer phase.

Although these observations and inferences add additional complications to the modeling of the kinetics and transport influences of this polymerization reaction, they resolve one of the fundamental polemics of reaction engineering of olefin polymerization. If the active catalyst is segregated at the periphery of the growing catalyst–polymer particles, transport limitations will not necessarily become increasingly significant as the polymerization yield increases. In industrial practice there is no indication of diffusion limitations throughout the polymerization process; however, characterization studies based on a uniform distribution of catalyst within the growing particle conclude that the process should become transport inhibited as the yield increases.

Acknowledgment. This work was conducted with the support of the National Science Foundation, renewal of Grant CTS 89-21381. Additional funding was provided by the Union Carbide Corp. The catalyst samples were provided by M. McDaniel from the Phillips Petroleum Corp. The tomography work was supported in part by the Processes and Techniques Branch, Division of Chemical Sciences, Office of Basic Energy Research, US DOE under Contract No. DE-AC02 76CH0016 (K.W.J., P.S.).

References and Notes

(1) Floyd, S.; Choi, K. Y.; Taylor, T. W.; Ray, W. H. *J. Appl. Polym. Sci.* **1983**, *32*, 2935.
(2) Chiovetta, M. G. PhD. Thesis University of Massachusetts, Amherst, MA, 1983.
(3) Webb, S. W.; Conner, W. C.; Laurence, R. L. *Macromolecules* **1989**, *22* (7), 2885.
(4) Schmeal, W. R.; Street, J. R. *AICHE J.* **1971**, *17* (5), 1188.
(5) Singh, D.; Merrill, R. P. *Macromolecules* **1971**, *4* (5), 599.
(6) Weist, E. L.; Ali, A. H.; Naik, B.; Conner, W. C *Macromolecules* **1989**, *22* (8), 3244.
(7) Sato, T.; Ikeda, O.; Yamakoshi, Y.; Tsubouchi, M. *Appl. Opt.* **1981**, *20*, 3880–3883.
(8) Carlsson, C. A.; Matscheko, G.; Spanne, P. *Med. Biol. Eng. Comput.* **1983**, *23*, Supplement 1.
(9) Carlsson, C. A.; Matscheko, g.; Spanne, P. *Biol. Trace Elem. Res.* **1987**, *13*, 209–217.
(10) Elliott, J. C.; Dover, S. D. *Metab. Bone Dis. Relat. Res.* **1984**, *5*, 219.
(11) Sequin, F. H.; Burstein, P.; Bjorkholm, P. J.; Homburger, F.; Adams, R. A. *Appl. Opt.* **1985**, *24*, 4117.
(12) Grodzins, L. *Nucl. Instrum. Methods* **1983**, *206*, 541.
(13) Flannery, B. P.; Deckman, H. W.; Roberge, W. G.; D'Amico, K. L. *Science* **1987**, *237*, 1439.

(14) Spanne, P.; Rivers, M. L. *Nucl. Instrum. Methods Phys. Res.* **1987**, *B24/25*, 1063.
(15) Spanne, P.; Rivers, M. L. *BioScience* **1987**, *1*, 101.
(16) Kinney, J. H.; Johnson, M. C.; Saroyan, R. A.; Bonse, U.; Nichols, M. C.; Saroyan, R. A.; Nusshardt, R.; Pahl, R.; Brase, J. M. *MRS Bull.* **1988**, *13*, 13.
(17) Kinney, J. H.; Johnson, Q. C.; Nichols, M. C.; Bonse, U.; Saroyan, R. A.; Nusshardt, R.; Pahl, R. *Rev. Sci. Instrum.* **1989**, *60* (7), 2471.
(18) Jones, K. W.; Bockman, R. S.; Gordon, B. M.; Rivers, M. L.; Saubermann, A. J.; Schidlovsky, G.; Spanne, P. Presented at the 2nd International Workshop on XRF and PIXE Applications in Life Sciences, Capri, Italy, June 1989.
(19) Jones, K. W.; Gorden, B. M.; Hanson, A. L.; Pounds, J. G.; Rivers, M. L.; Schidlovsky, G.; Smith, J. V.; Spanne, P.; Sutton S. R. *Microbeam Analysis*; Russell P. E., Ed.; San Francisco Press: San Francisco, CA, 1989; pp 191–195.
(20) Jones, K. W.; Gordon, B. M.; Hanson, A. L.; Pounds, J. G.; Rivers, M. L.; Schidlovsky, G.; Smith, J. V.; Spanne, P.; Sutton, S. R. *Microbeam Analysis*; Russell, P. E., Ed.; San Francisco Press: San Francisco, CA, 1989.
(21) Nichols, M. C.; Kinney, J. H.; Johnson, M. C.; Saroyan, R. A.; Bonse, U.; Nusshardt, R.; Pahl, R. *Rev. Sci. Instrum.* **1989**, *60* (7), 2475.
(22) Sakamoto, K.; Suzuki, Y.; Hirano, T.; Usami, K. *Jpn. J. Appl. Phys.* **1988**, *27* (3), 127.
(23) Jones, K. W.; Bookman, R. S.; Gordon, B. M.; Rivers, M. L.; Saubermann, A. J.; Schidlovsky, G.; Spanne, P. Proceedings of the 2nd International Workshop on XRF and PIXE Applications in Life Sciences, Capri, Italy, June 1983.
(24) Spanne, P. *Phys. Med. Biol.* **1989**, *34* (6), 679.
(25) Webb, S. W. Ph.D. Thesis, Department of Chemical Engineering, University of Massachusetts, Amherst, MA, 1990.